Eidgenössische Technische Hochschule Zürich
Swiss Federal Institute of Technology Zurich

Empa
Materials Science and Technology

Sensitivity Analysis of Melt pool Dimensions and Optimization of modeling Parameters using SLM thermal Single-Track Simulations of Hastelloy X

Bardh Dervishaj

Semester Project

08.11.2021

Prof. Dr. Edoardo Mazza

Dr. Ehsan Hosseini

Pooriya Gh Ghanbari

Abstract

Additive Manufacturing (AM) is a modern and promising manufacturing technique which can produce highly complex and adaptable structures. AM has struggled to find commercial success due to the lack of general understanding and is therefore heavily researched. The focus in research is to capture the full complexity of AM and be able to reproduce the process in the virtual world while minimizing the computational cost. For this task virtual models have been developed that promise to deliver representative results. In this project a sensitivity analysis of melt pool dimensions to process and modeling parameters was performed. For this purpose, multiple Design of Experiment (DOE) approaches were employed, and their performances were compared. Additionally, the Response Surface Method (RSM) was applied to validate the claims from the sensitivity analysis and to find a second order representation of the system. In a last step an optimization was performed on the Response Surface to predict optimal values for the modeling parameters.

Eidgenössische Technische Hochschule Zürich
Swiss Federal Institute of Technology Zurich

Declaration of originality

The signed declaration of originality is a component of every semester paper, Bachelor's thesis, Master's thesis and any other degree paper undertaken during the course of studies, including therespective electronic versions.

Lecturers may also require a declaration of originality for other written papers compiled for theircourses.

I hereby confirm that I am the sole author of the written work here enclosed and that I have compiled itin my own words. Parts excepted are corrections of form and content by the supervisor.

Title of work (in block letters):

Sensitivity Analysis of Meltpool Dimensions and Optimization of modeling Parameters using SLM thermal Single Track Simulations of Hastelloy X

Authored by (in block letters):

For papers written by groups the names of all authors are required.

Name(s):	**First name(s):**
Dervishaj	Bardh

With my signature I confirm that

- I have committed none of the forms of plagiarism described in the 'Citation etiquette' informationsheet.
- I have documented all methods, data and processes truthfully.
- I have not manipulated any data.
- I have mentioned all persons who were significant facilitators of

the work.I am aware that the work may be screened electronically for

plagiarism.

Place, date	**Signature(s)**
08.11.2021	Bar. Dervishaj

Contents

List of Figures

List of Tables

1

1 Introduction

1.1 Motivation

The demand of adaptable and flexible structures has led to development of manufacturing processes that can produce highly complex parts. Therefore, new manufacturing techniques like Additive Manufacturing (AM) are being heavily studied and promise to be the solution to this problem. Additive Manufacturing opens the possibility of manufacturing parts with high complexity while requiring minimal additional effort. One of the major drawbacks of these techniques is that the material needed for most processes needs to be present in powder form. This increase the material cost substantially and is one of the main reasons why AM hasn't found commercial success yet. Contemporaneously, AM parts have had a history of worse structural performance when compared to their conventionally manufactured counterparts.

One of the main subcategories of Additive Manufacturing is Selective Laser Melting (SLM). Selective Laser Melting is a layer-based manufacturing technique that aims to produce complex part while minimizing the amount of waste. SLM achieves this by trying to optimize the usage of material during the process and only use material for the part and its supports. With this procedure material is only added to the part and never removed, giving these techniques the name "Additive Manufacturing". The drawback of this technique is that the process is not fully understood yet. Therefore, recent studies have focused on the

development of sophisticated, predictive models which promise to capture the procedure in its full complexity. This would simplify the integration of AM into the manufacturing pipelines of companies and open a new chapter for commercial manufacturing.

1.2 Objective of this Project

The SLM process can be divided into smaller subprocesses, namely: Material deposition, Mel pool formation and Solidification. To understand the SLM process each of these segments must be fully understood separately. Therefore, the focus of this project lies on the central part of SLM, which is the melt pool formation.

To contribute to the understanding of the SLM process, this project aims at characterizing the sensitivity of the melt pool dimensions (depth and width) to process and modeling parameters (heat source parameters and material absorptance). In a later step the chosen modeling parameters were optimized for a given set of process parameters.

For the quantification of melt pool dimensions a fully automated MATLAB tool was developed. This MATLAB tool runs thermal simulations in ABAQUS, extracts the thermal data and computes the melt pool dimensions directly.

2

2 Theoretical Basics

2.1 Material: Hastelloy X

After the invention of the gas turbine engine, it was evident that the overall efficiency of these engines was limited by the peak temperature they could operate at. To illustrate this, a simplified thermo dynamic cycle, also known as the Brayton Cycle, can be found in figure 2.1. In the first step of this thermodynamic cycle, gas is taken in at atmospheric pressure and temperature (1). In the following steps the gas is compressed to a higher pressure (2) and combustions occurs, raising the temperature of the chamber to its peak value (3). Afterwards, the gas is expanded back to a lower level of pressure and temperature (4), which produces work that can be extracted to drive the turbine. A simplified version of the thermodynamic efficiency of this system can be expressed as follows [1]:

$$\eta_{\mathrm{th}} = 1 - \frac{T_4}{T_3}$$

Where T_4 is the peak temperature of the chamber and T_3 is the temperature of the released gases. From this formulation it is evident that to increase the thermodynamic efficiency either T_3 must be decreased or T_4 must be increased. Since T_3 is difficult to control it is much simpler to increase T_4 [1]. This put new requirements on existing materials, which encouraged the development of Nickel

base alloys that exhibit high strength at elevated temperatures and high oxidation resistance. One of these Nickel based superalloys is Hastelloy X.

The nominal chemical composition of Hastelloy X can be found in Table 2.1.

Element	Ni	Fe	Cr	Co	Mo	W	C	Si	Mn
Composition [%]	Bal.	18.2	21.5	2.1	9.4	0.9	0.04	0.5	0.1

Table 2.1 : Nominal chemical composition of Hastelloy X [30]

Hastelloy X is known for being a Solid-Solution strengthened Nickel base superalloy which forms Mo-rich carbides when exposed to short thermal energy [2], while long exposure leads to formation of detrimental phases like μ and σ [4].

One of the main drawbacks of Hastelloy X in combination with SLM is its susceptibility to hot cracking during the manufacturing process. Due to the rapid cooling rates in SLM, Hastelloy X samples usually form a columnar dendritic microstructure [3]. Samples build with SLM tend to have higher yield strength (YS) and ultimate tensile strength (UTS) and lower elongation properties when compared to hot forged samples. This can be attributed to the ultrafine microstructure that develops during the SLM process [6].

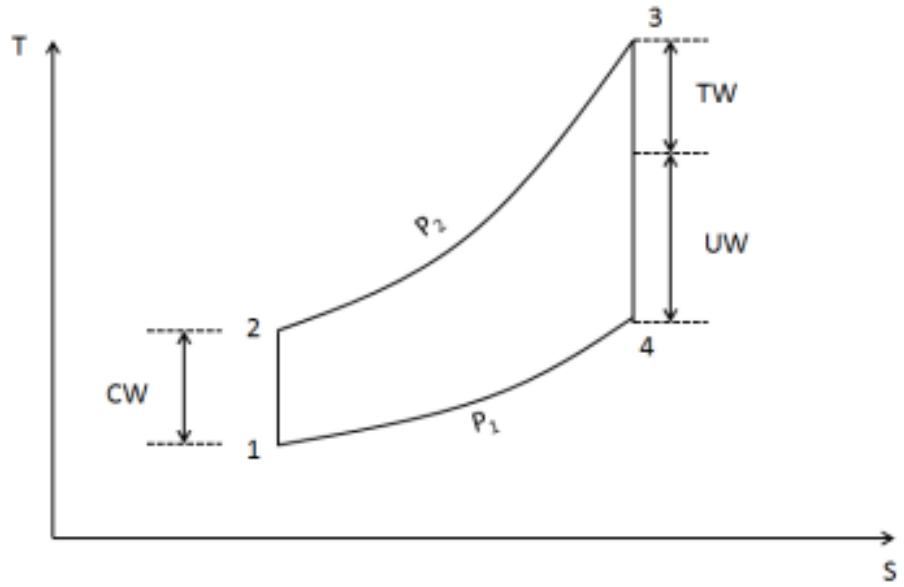

Figure 2.1 : Entropy-Temperature Diagram for the Brayton Cycle [1].

2.2 Selective Laser Melting (SLM)

Selective Laser Melting is a layer-based powder bed manufacturing technique in which selective areas of a powder layer are molten into a fully connected part. A representation of the SLM process can be found in **figure 2.2**. The SLM process starts by creating a model of the desired part in a CAD software. In the next step the support structures are added to the model. Since SLM parts are produced Layer by Layer, overhanging structures need to be sufficiently supported, to ensure stability during manufacturing. After this step the model is sliced into equally thick layers which will later be used as the blueprint for the SLM process. Then the model data is loaded onto the SLM machine, and the manufacturing process can begin.

First, the build platform is lowered by one layer thickness and the powder delivery platform is raised to provide material for the recoater. In the next step, the recoater is moved across the build platform to apply a layer of powder. Then, the moving mirror redirects the laser to the start position and the laser source is turned on. From now on the moving mirror will read out the current layer information from the model data and redirect the laser to the correct positions. While the laser is moving across the build plate it will melt the powder on the laser path and create a connected surface. After the laser has fully molten all selective areas of this layer, the laser is turned off and the process is repeated until the part is fully manufactured.

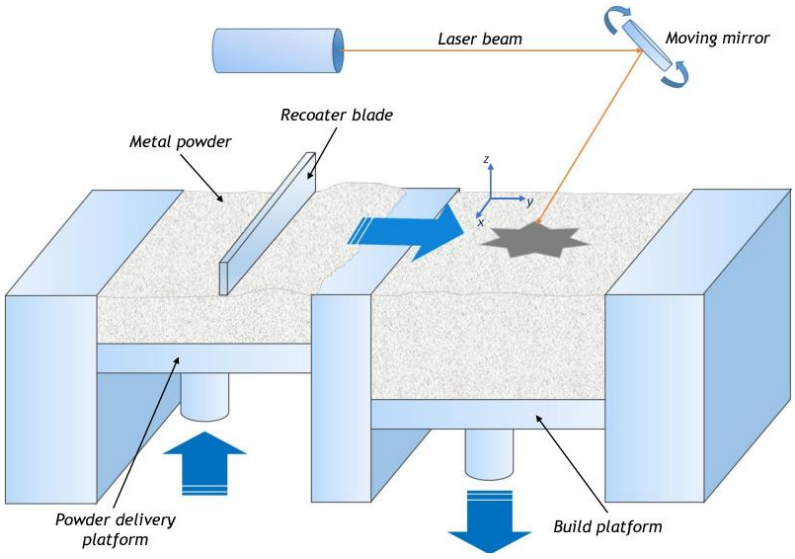

Figure 2.2 : Schematic representation of the SLM process.

Parts produced with this process tend to have microcracks, pores and poor surface quality. To increase the mechanical quality of the part, postprocessing is performed. The first step in postprocessing is detaching the part from the build plate and removing the support structures from the part. In a next step the part's surface is machined and polished. This increases the part's fatigue performance as fatigue cracks usually nucleate from the surface and use surface imperfections as crack nucleation sites.

The defects in SLM can be subdivided into two main categories, namely Lack of Fusion defects (LoF) and Keyhole Pores. Lack of Fusion defects form when the powder layer is not fully molten, which leads to partially connected layers and is detrimental to the part's quality. In postprocessing Hot Isostatic Pressing (HIP) is performed to counteract these LoF defects by compressing the part at an elevated temperature, which leads to better bonding of the partially connected layers. Contrary to LoF defects Keyhole pores cannot be removed by Hot Isostatic Pressing. These pores form during the SLM process when the energy input is high. Due to this high energy input the material reaches boiling point and starts to evaporate, which creates an evaporation pressure that depresses the melt pool. This depression creates new melt pool surface deep inside the melt pool at which laser energy is constantly being reflected and absorbed, encouraging further evaporation of the material. A schematic representation of this effect can be found in figure 2.3.

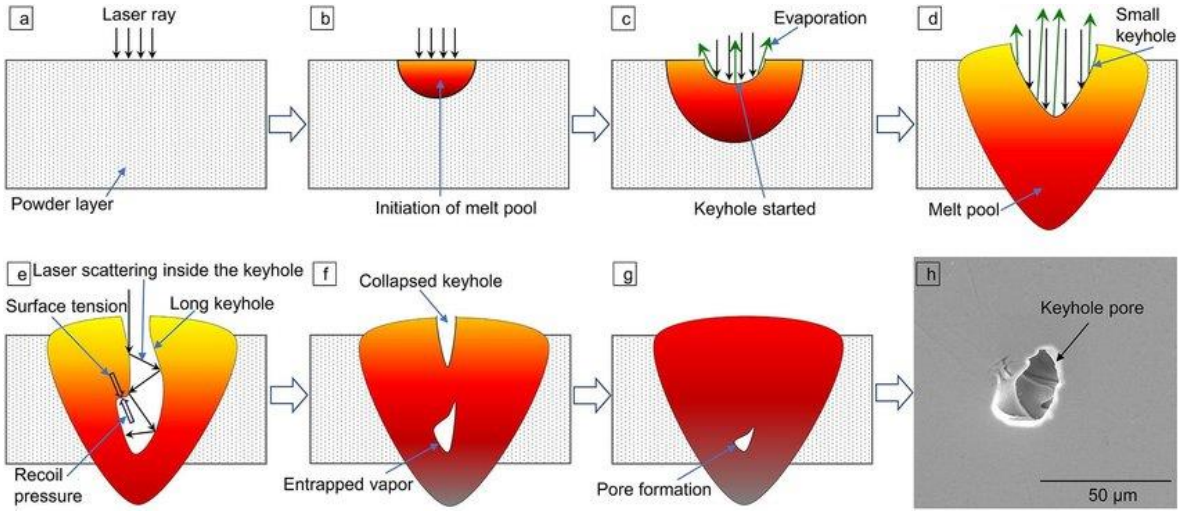

Figure 2.3 : Schematic representation of the formation of LoF defects and Keyhole pores. [10]

If the keyhole depression is still present when the solidification occurs a keyhole pore is formed. These pores can be distinguished between the LoF defects by their shape since keyhole pores are usually present in a spherical shape while LoF pores have irregular shapes. Keyhole pores are considered to be dangerous and detrimental to the part's quality, since they contain high pressure gas. Simultaneously, it is difficult to predict the mechanical response of a part with Keyhole pores or remove the Keyhole pores with postprocessing. Therefore, studies like W. E King [8] are trying to quantify the formation of Keyhole pores in SLM. King suggests the following estimation for the formation of Keyhole pores in 316L stainless steel samples using the normalized enthalpy:

$$\frac{\Delta H}{h_s} > \frac{\pi * T_b}{T_m}$$

Where ΔH is the specific enthalpy, h_s enthalpy at melting, T_m the melting temperature and T_b the boiling temperature of the material.

2.3 SLM Process Parameters and Energy Density

Due to its complexity and high dimensionality, the SLM process is attempted to be explained with models that minimize the number of parameters. It is desired that this set of parameters is material independent and fully captures the complexity of the system. Hence, the main parameters in SLM are chosen to be as follows:

- P: Laser Power $[W]$
- v_s: Scan Speed $[\frac{mm}{s}]$
- t_s: Layer Thickness $[mm]$
- h: Hatch Distance $[mm]$
- Scan Strategy

These parameters are used to characterize and predict the quality and efficiency of a SLM process.

Another method, which combines the previously mentioned process parameters, is called the energy density method, in which one global energy density parameter

is used as the main parameter of the system. This has proven to be a good starting point in the analysis of SLM processes and has been widely used in research.

The dimensions of this energy density are application dependent and can vary between three main definitions. These three definitions consist of the following [1]:

- Specific three-dimensional Energy Density: $E_v = \frac{P}{v_s * t_s * h}$ $\left[\frac{J}{mm^3}\right]$
- Specific two-dimensional Energy Density: $E_v = \frac{P}{v_s * h}$ $\left[\frac{J}{mm^2}\right]$
- Specific one-dimensional Energy Density: $E_L = \frac{P}{v_s}$ $\left[\frac{J}{mm}\right]$

L. Carter [1] suggests another definition for the three-dimensional energy density, namely:

$$(E_v = \frac{P}{v_s * d_L * h})$$

Where d_L is the laser spot size. All these definitions try to give an estimation of the input energy, since this has proven to be an important quantity for the prediction of SLM processes.

3

3 Methods and Modeling

In this chapter an explanation of all modeling techniques and methods used in this project will be given. Additionally, the setup of the simulation environment and the assumptions made will be described in detail.

3.1 Heat Source Model (Goldak)

The governing equation of the SLM process can be represented by the following equation [11]:

$$\frac{dH}{dt} = \nabla * q(r,t) + Q(x,y,z,t) \quad in\ \Omega$$

$$with\ q = -k * \nabla T$$

Where $\frac{dH}{dt}$ is the enthalpy derivative with respect to time t, q is the heat flux vector, Q is the heat source term, k is the conduction term of the material, T is the temperature and Ω is the domain of the body. As evident from this formulation a good approximation of the term q and Q are essential for a simulation to be representative of the process. To represent Q an adequate heat source model must first be chosen.

In practice there are two main categories of heat source model, namely surface heat sources models and volumetric heat sources models. Surface heat source models are generally used for interface tracking, where the heat source acts on the surface of the melt pool, after the powder layer has been molten by a volumetric heat source [11]. If Surface heat sources are used as the only heat source in a SLM simulation, then they tend to produce a concentrated heat flux

on the surface of the powder layer which leads to a localization of thermal energy at the surface of the powder. Due to this localized energy, vaporization can easily occur in the vicinity of the laser spot. This behavior is reinforced by the low conductivity of the powder layer and is the reason why surface heat sources are known for overpredicting the vaporization in the SLM process. Surface heat sources also do not take the laser penetration into the powder layer into account. One way to work around this issue is by implementing methods like the ray tracing method, where the surface heat source is modeled as a laser source with outgoing laser beams. The model then tries to represent the path of the laser beam deep into the powder layer, considering all reflections of the laser beam on the surface of the powder particles. This approach is computationally expensive and requires a particle-based model of the powder layer but is capable of producing representative results when compared to experimental data [13].

The main advantage of volumetric heat sources is that they can capture this laser penetration even when the powder is modeled as a continuum. At the same time volumetric heat sources are easy to implement in commercial software like ABAQUS and tend to predict the melt pool dimensions with high accuracy, while being computationally less expensive than the ray tracing methods [11]. One disadvantage of volumetric heat source models is their inability to accurately predict vaporization in the powder layer. Volumetric heat sources spread the thermal energy in a wide three-dimensional domain which attenuates the temperature concentration in the vicinity of the laser spot. This leads to lower peak temperatures in simulations that use volumetric heat sources as compared to simulations that use surface heat sources [11].

Because of its simple implementation in commercial software, its low computational cost and since vaporization phenomena were ignored the volumetric heat source model was chosen for this project.

The volumetric heat source chosen in this thesis is the Goldak heat source model. The Goldak power density distribution for the rear (r) and front (f) part of the heat source model can be defined by the following equation [14]:

$$Q_{f/r}(x,y,z) = \frac{6\sqrt{3}f_f Q}{abc_{f/r}\pi\sqrt{\pi}} \exp\left(\frac{-kx^2}{a^2}\right)\exp\left(\frac{-ly^2}{b^2}\right)\exp\left(\frac{-mz^2}{c^2}\right)$$

Where Q is the energy input rate, $(a, b, c_{r/f})$ are the geometrical Goldak modeling parameters, (k, l, m) are the concentration factors in each direction.

From this equation it is apparent, that the Goldak model is a double ellipsoid heat source model with exponentially decaying power density distribution along the main directions. A schematic representation of the Goldak heat source model can be found in **figure 3.1**. To limit the number of parameters in the analysis c_f was chosen to be equal to a.

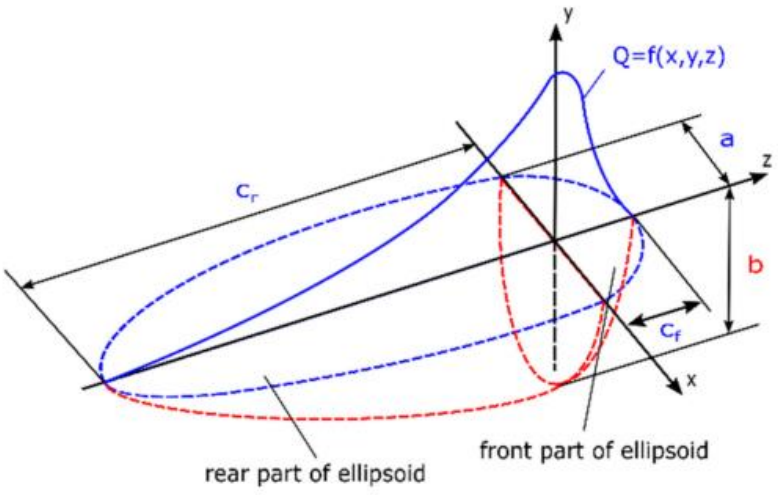

Figure 3.1 : Goldak Heat Source Model. [12]

3.2 Powder Modeling

As previously mentioned, a proper modeling of the powder layer is crucial to ensure the correctness of results. Since powder is a porous medium it is not expected for powder to have the same material properties as the bulk material. The thermal conductivity of powder varies in the range of 1.5%-1% of the thermal conductivity of bulk material. This can be attributed to the heavily reduced contact surface between powder particles as compared to the bulk material, which attenuates the transmission of thermal energy through the medium. The low thermal conductivity of the surrounding gas causes thermal energy transfer to be mainly driven by the contact surface of the particles [16]. When modeling thermal conductivity an assumption for the directional dependence must be made. K. Lee [11] suggest that there is a non-negligible directional dependence and proposes an anisotropically enhanced thermal conductivity. For this thesis an isotropic thermal conductivity model was chosen, due to its simple implementation.

Oppositely, powder tends to have higher absorption properties when compared to bulk material, which can be explained by a general laser path. As a laser beam hits the surface of a powder particle some of its energy is absorbed while the rest is reflected. This reflected beam can then travel through pores in the medium and hit other powder particles where part of its energy is absorbed, and the rest is reflected again. This continues until the laser beam leaves the powder layer or until the laser beam's energy has been fully absorbed. The absorption coefficient is usually set to be temperature dependent but isotropic. There are studies that suggest a depth dependence of the absorption coefficient [11]. For this project a constant and isotropic absorption coefficient was chosen for the powder layer.

A summary of the chosen thermal conductivity can be found in the following table:

Thermal Conductivity		
Thermal Conductivity $[\frac{W}{mK}]$	Temperature $[°C]$	Field
9.1	25	Bulk
34	1260	Bulk
0.124	25	Powder
0.169	1260	Powder

Table 3.1 : Thermal Conuctivity of powder and bulk material used in the thermal simulation.

With this, there are two main options for powder modeling in the context of SLM, namely the continuum-based and particle-based modeling. As previously mentioned, the particle-based modeling approach is computationally expensive but can produce accurate results. In this approach the powder layer is represented by a selection of randomly oriented and shaped powder particles. This technique can be used with either surface or volumetric heat source models but tends to find most success in conjunction with surface heat sources when paired with ray tracing methods [13]. Since the mesh for this thesis had already been created and optimized, figure 3.2, a continuum-based approach was chosen. In this approach the whole powder layer is replaced by a continuum with powder properties.

Advantages of this approach are low computation times and elimination of any randomness that might occur when sampling the powder particles in the particle-based approach. To keep track of which part of the simulation is powder and which part is bulk, a field variable was introduced. This field variable is 1 if the current element is bulk material and 0 if the current element is powder. In the initialization step this field variable is set to be 0 in the powder layer and 1

everywhere else on the mesh. A subroutine keeps track of all elements that have surpassed their melting temperature (here $T_m = 1285\ °C$) and replaced their field variable with 1. The mesh and a possible result after completion of a thermal simulation can be found in **figure** 3.2.

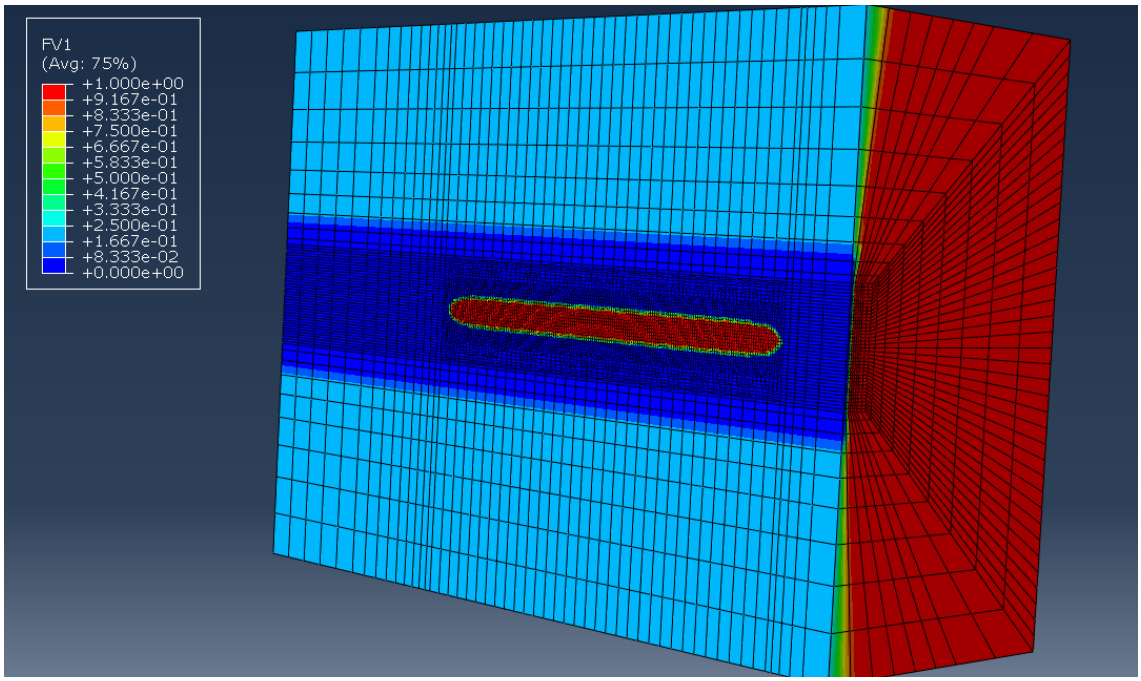

Figure 3.2 : Results of a thermal simulation showing the evolution of the field variable.

3.3 Design of Experiments (DoE)

To capture the full complexity of a multidimensional system (like SLM) Design of Experiments methods are often applied. These methods act as a tool to sample experimental/simulation data points in the design space of the system. The goal of these methods is to decrease the number of experiments/simulations that must be performed in order to get a representative model of the system. They are often used in direct optimization, sensitivity analysis or for the creation of a start generation in genetic algorithms. In research a large amount of Design of Experiment techniques are used to varying success [17].

3.3.1 One-Factor-at-a-Time (OFAT)

One of the most used DoE methods is the One-Factor-at-a-Time Design. OFAT design is part of the family of systematic sampling techniques in which the sampling of the same system is always going to be the same. The counterpart to this are stochastic sampling methods, in which design points are sampled with a random component.

The main appeal of this DoE is its simple implementation and its ability to produce results in a swift manner. In this DoE only one factor at a time is changed between experiments/simulations. This is supposed to give an accurate representation of the system's dependence on the specified parameter. Since only one parameter is changed between simulations the results become simple to analyze and conclusions can be drawn in a fast pace. The predictive capabilities of this sampling techniques tend to underperform when compared to other DoE because OFAT is incapable of predicting the interaction between different parameters [19]. Furthermore, optimization with this technique, see **figure 3.3**, is difficult since only one parameter can be optimized at a time. This can make the optimization either slow or sometimes impossible.

Considering everything, OFAT design can be considered as an efficient sampling strategy to get a first understanding of the system's response but is not sophisticated enough to fully explain the complexity of most multidimensional systems. For this reason it was decided against using an OFAT design in this project.

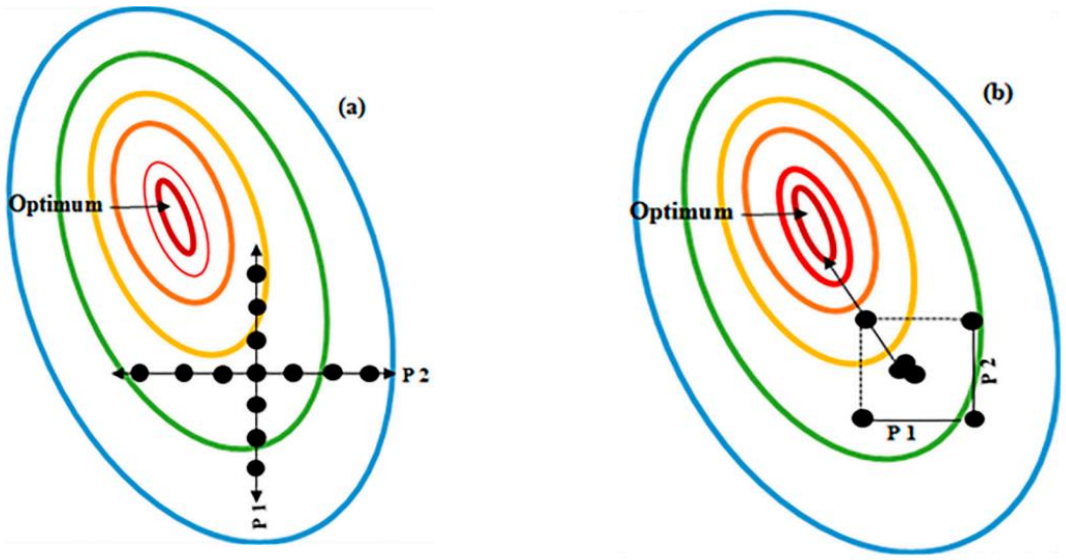

Figure 3.3 : Schematic representation of an optimization process using (a) OFAT design and (b) D-optimal design.

3.3.2 Full Factorial Design

The Full Factorial Design is commonly used in research since it promises to cover most of the system's design space. It does this at the cost of efficiency by covering every possible combination of parameters in experiments/simulations. For this Design to be implemented the continuous parameters of the design space must first be discretized into a number of discrete values, called levels. If the number of levels of each parameter are identical, the design is called Symmetric Factorial Design else it is called Asymmetric Factorial Design. The number of experiments that are needed for a symmetric full factorial design can be calculated using the following relation [20]:

$$\#Experiments = n^k$$

While for an asymmetric design the following holds [20]:

$$\#Experiments = \prod_k n_i$$

Where n_i is the level of the current parameter and k is the number of parameters in the system. As evident from this formulation, the number of experiments that need to be performed scales exponentially with the number for levels and the number of parameters. Therefore, it is often advised to only use this method with a two-level design when the number of design parameters is lower than 6. To circumvent this problem other methods like Fractional Factorial Design have been developed. In this design a subset (fraction) of design points in the Full Factorial Design are chosen such that this subset still satisfies the sparsity-of-effects principle. The sparsity-of-effects principle states that not all effects are statistically significant and that the system's response is driven by the main effects and some low order interaction terms [21].

One of the main advantages of the Full Factorial Design is the ability to predict the influence of interaction terms between parameters. The reason for this is that two arbitrary simulations in the DoE are likely to have multiple varied parameters between them, which opens room for the interpretation of the interaction terms between these parameters.

As previously stated, the Full Factorial Design is good at predicting the system's sensitivity to parameters when the parameter count is low. In the context of SLM it was decided to implement this in the melt pool sensitivity analysis to process parameters. For the main process parameters, it was decided

to investigate the influence of Laser power P, Scan Speed v and Layer Thickness t. Furthermore, the Factorial Design is set to be asymmetric in order to be consistent with the parameters of the experiments that will be conducted later. A tabular representation of the investigated discrete values for these process parameters can be found in the following table:

Laserpower [W]	Scan Speed $[\frac{mm}{s}]$	Layer Thickness $[\mu m]$
150,175,200	700,900,1100	0,20,30,40

Table 3.2: Process Parameters studied in the meltpool sensitivity analysis.

3.3.3 Central Composite Design

The Central Composite Design is traditionally used in conjunction with metamodeling techniques like the Response Surface Method, which will be discussed in detail in **chapter 3.4**. The first step in this design is to select representative parameter ranges for each design parameter of the system. These ranges should be carefully chosen since the Central Composite Design will impose additional constrains on them. In a first step the corner points are added at the extrema of the parameter ranges, which serves as foundation and is called factorial pre-design. In the next step the star points are added to the design. The position of these points can be determined by considering the type of the chosen Central Composite Design [22].

There are three main types of the Central Composite Design, namely Circumscribed (CCC), Inscribed (CCI) and Face Centered (CCF) Designs. For a graphical representation of each design type refer to the following figure.

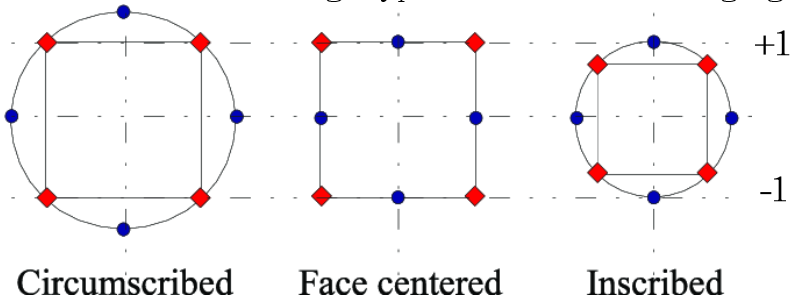

Figure 3.4 : Representation of the three main types of Central Composite Design with blue dots representing the corner points and red dots representing the start points. [22]

As evident from the above figure the star points for a Circumscribed design lie outside of the predefined parameter range. The distance from the star points to the center is exactly α.

According to [22] α can be calculated for each factorial pre-design using the following relation:

$$\alpha = [number\ of\ factorial\ runs]^{\frac{1}{4}}$$

This sampling guarantees that the design points lie on a multidimensional sphere and thus have the same distance from the center point. This type of DOE is called Rotatable Design. The rotatability of a design promises that the prediction variance of the metamodeling technique used in conjunction with that design approach is only a function of the multidimensional radius. This definition for the start points of a Circumscribed Design poses new restrictions on the selection of the parameter range, since it samples design points outside of that range. If the factorial design was set out to be the entire physical domain of a parameter (e.g., Laser powder from [0W-250W]) then the Circumscribed Design would impose unphysical design points (e.g. [-50W]).

These are the reasons why the other design types were developed. In the Face-Centered approach the star points are positioned at the center of each face in the factorial space [22]. This whole design then acts as an enhanced full factorial design and is used in situation where the parameter ranges are fully constrained and can’ t be changed but the Circumscribed design would lead to unphysical design points.

The Inscribed Design tries to mimic the properties, like rotatability, of the Circumscribed design type while also not sampling design points outside of the predefined parameter ranges.

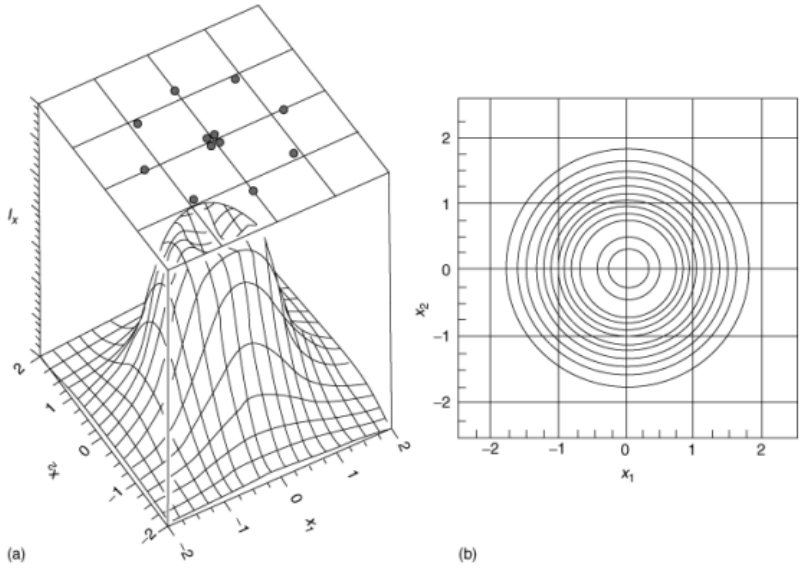

Figure 3.5 : (a) Circumscribed Design depicting the inverse of the prediction variance as a function of Desing Parameter x1 and x2 and (b) contours of the variance showing rotatibility of the desing. [23]

3.3.4 Latin Hypercube Design

The Latin Hypercube Design was developed in 1979 by Michael McKay as an optimized method to sample design points for computer experiments [24]. The promise of this method is its ability to cover the entire design space with a low amount of design points and still be capable of producing representative results. This design is known as a stochastic sampling method where the position of a design point is partially evaluated by a random component. The main property of stochastic sampling methods is their ability to create different designs even when considering the same parameter and parameter ranges. The deviations between these designs can reveal more nuanced attributes of the system when multiple DoEs are performed on the same system.

In the Latin Hypercube approach the design space of a given system is divided into equally sized intervals. In a next step, uniqueness of parameter values is enforced, meaning that parameter can only take discrete values corresponding to the value of any interval. Each interval value is only allowed to be present once in the whole Latin Hypercube Design. This is done by giving each set of parameters the same probability of being picked and picking random parameter sets while not overlapping parameters with same values. This sampling allows an estimation of the main effects of the system in an unbiased manner. The Latin Hypercube Sampling thus provides the following sample matrix [26]:

$$S_{ij} = \frac{\eta_{ij} - \xi_{ij}}{P} \quad i = 1 \dots P \,, j = 1 \dots n$$

Where P denotes the number of points, n is number of intervals of the parameters, η_{ij} are uniform random permuatations of the integers 1 to P and ξ_{ij} are independent random numbers uniformly distributed between 0 and 1. A commonly used simplified version of the above definition is the Latin Hypercube Design with centered points of P equal-probability sub-intervals [26]:

$$S_{ij} = \frac{\eta_{ij} - 0.5}{P} \quad i = 1 \dots P \,, j = 1 \dots n$$

If the Latin Hypercube Design would be implemented only using the above mentioned restriction nothing would stop the design from creating samplings that don’t fully explore the entire design space (e.g. Diagonal Design), see figure 3.6. To further optimize the choice of design points other algorithms, like the max-min algorithm, were implemented. In the max-min algorithm the Latin Hypercube

sampling and an optimization algorithm that tries to maximize the minimum distance between any two points are run simultaneously.

By implementing this secondary optimization technique, it is ensured that the generated Design of Experiments can fully cover the design space with very few design points and yield results that can capture most of the complexity of the given system.

For this project a Latin Hypercube Design was chosen to create thermal simulation design that was later used for metamodeling using Response Surface Method. This method was run in conjunction with a max-min optimization algorithm to ensure good space filling properties of the sampling. The results and performance of this procedure can be found in chapter 4.5.

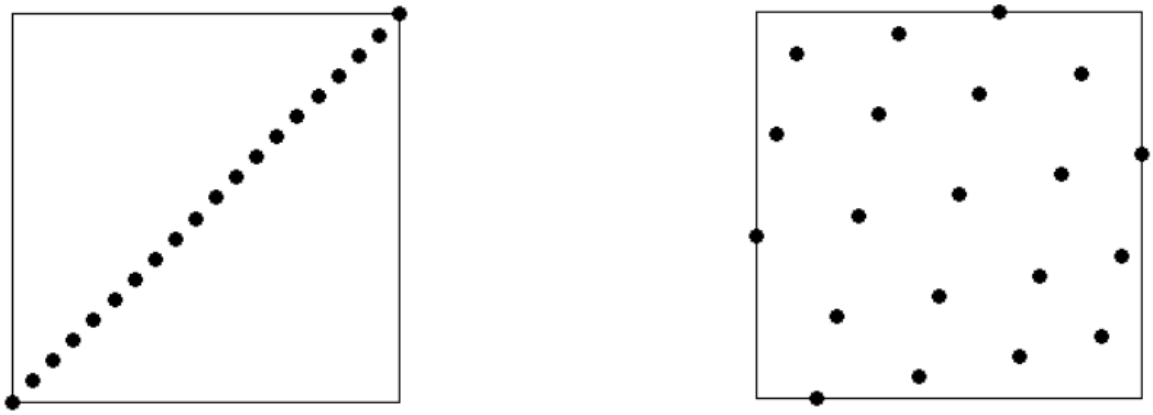

Figure 3.6 : (a) Two dimensional design space with poor space filling properties and (b) with good space filling properties, sampled using Latin Hypercube Design. [25]

3.4 Response Surface Method (RSM)

According to Myers [27] the response surface method is "a collection of statistical and mathematical techniques for developing, improving and optimizing processes". RSM has been widely used in research to create metamodels, which are then used to predict a system's response for a given set of initial and boundary conditions. One of the main advantages of RSM is that it tries to find a low order (usually 1-3 order) model that represents the given dataset, by minimizing the mean squared error of the data. This makes the implementation of RSM rather simple while not losing predictive accuracy when compared to other metamodeling techniques.

Before using RSM to find a metamodel, first a predetermined design set is required. This design set should be generated using DoE methods and should cover most of the design space. At the same time RSM does not require a large amount of design points to find a solution for the model. Therefore, it is often used in combination with design point minimization techniques like Latin Hypercube Design, Central Composite Design or D-Optimal Design, which is not covered in this project.

RSM is often used in cooperation with optimization techniques, because of the smoothness of its response surface. The smoothness of the response makes optimization simple and tends to approximate the global extrema of the system, since smoothing can get rid of localized information, like local extrema. At the same time, it is difficult for RSM to predict extrema of a system if the system's true response has large gradients in the vicinity of the extrema. Therefore, a smart choice of design points (DOE) is essential to the success of the RSM. For a schematic representation of the RSM method and its optimization see figure 3.7.

Since RSM, even with application of design point minimizing techniques, requires a good coverage of the whole design space it is not advised to use RSM in systems with high parameter count (>15). If this situation arises it is suggested to limit the amount of design parameters by either neglecting certain parameters that have low influence on the system or by using methods like the Principal Component Analysis (PCA) to find the main components of the system.

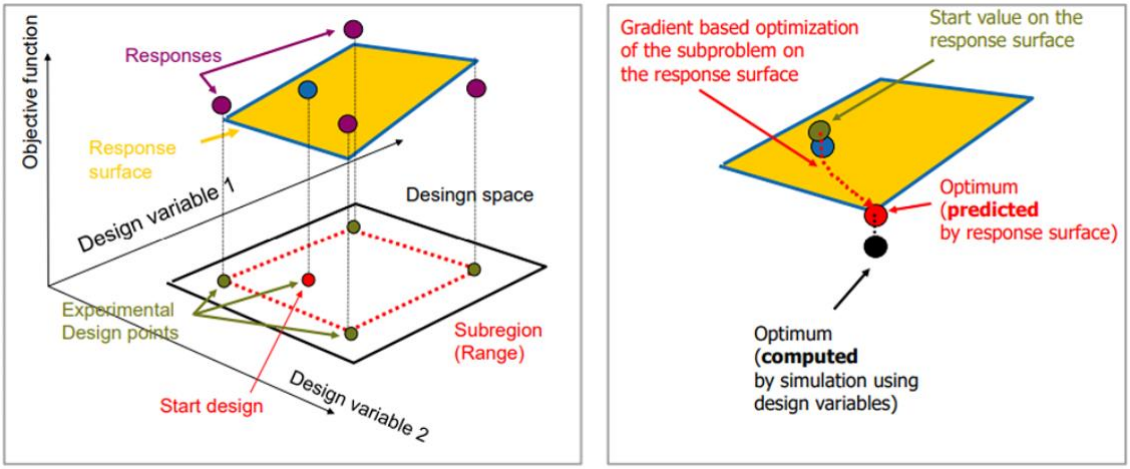

Figure 3.7 : (left) DOE desing points sampling and Response Surface fitting and (right) optimization on the generated Response Surface. [26]

In this project the Response Surface Method was applied together with the sampling strategies of Latin Hypercube Design as well as Central Composite Design. To verify the correctness of the response surface an error analysis was performed. This error analysis was divided into two main parts. The first part tries to compare the prediction error of the model by training the model on a fraction of the dataset and using the remaining part of the dataset as a testing set for the model. The residual sum of squares can then be calculated as:

$$\varepsilon_{pred} = \sum_{i=1}^{B} (y_i - \hat{y}_i)^2$$

Similarly, a second approach for the error estimations was implemented, namely the coefficient of multiple determination R^2. This error can be calculated using the following relation:

$$R^2 = \frac{\sum_{1=1}^{P} (\hat{y}_i - \overline{y}_i)^2}{\sum_{1=1}^{P} (y_i - \overline{y}_i)^2}$$

Where B denotes the number of points in the testing set, P the number of design points, $\hat{y}_i$ denotes the predicted response, y_i the actual response and $\overline{y}_i$ the mean of the responses.

4

4 Results and Discussion

In this chapter a summary of all results and their analysis will be presented. These results consist of thermal simulation results of 220 simulations that were simulated using the commercial software ABAQUS. In a first step, a brief explanation of data acquisition is presented. Followed by the sensitivity analysis of melt pool dimensions to process parameters. Afterwards, the results of the sensitivity analysis to modeling parameters will be illustrated. Following this, the optimization results of the model parameters will be shown.

4.1 Result Extraction

For the results acquisition a fully automated MATLAB tool was developed which is capable of running virtual experiments based on a DOE spreadsheet. It does this by integrating the desired parameters from the DOE sheet into the simulation and running that simulation in ABAQUS. For simplified implementation of AM simulations in ABAQUS the AM-toolbox was used. After the successful completion of the simulation, the MATLAB tool will read out all relevant data from the generated .dat, .sta and .odb file. With this thermal data, the MATLAB tool can start extracting the melt pool dimensions. It does this by looping through the data for each timestep and determining a convex hull of the melt pool (Nodes with temperature higher than their respective melting temperature). This is a first approximation of the melt pool dimensions. Later in the project it was decided that this approach oversimplifies the melt pool dimensions by being limited to the element size (results can only occur in discretized steps). Therefore, it was decided to interpolate between nodes to get a more representative value for the melt pool dimensions. For the temperature definition of the internodal

temperature a linear shape function was used. This approach has proven to provide a more accurate representation of the melt pool dimensions. Furthermore, the melt pool dimensions were averaged across the intermediate heating time steps. This ensures that outliers in the melt pool dimension analysis don't have large impact on the solution.

Here, it is worth noting that for a quantification of melt pool dimensions it was explicitly decided to not take melt pool length into account. This is partially because reliable experimental data on melt pool length is difficult to find, since melt pool length is generally hard to measure in experiments.

Additionally, this MATLAB tool was developed together with Burim Dervishaj, who was doing his Semester Thesis in the field of microstructure sensitivity analysis in the context of SLM.

For a schematic representation of the tool's workflow see **figure 4.1**.

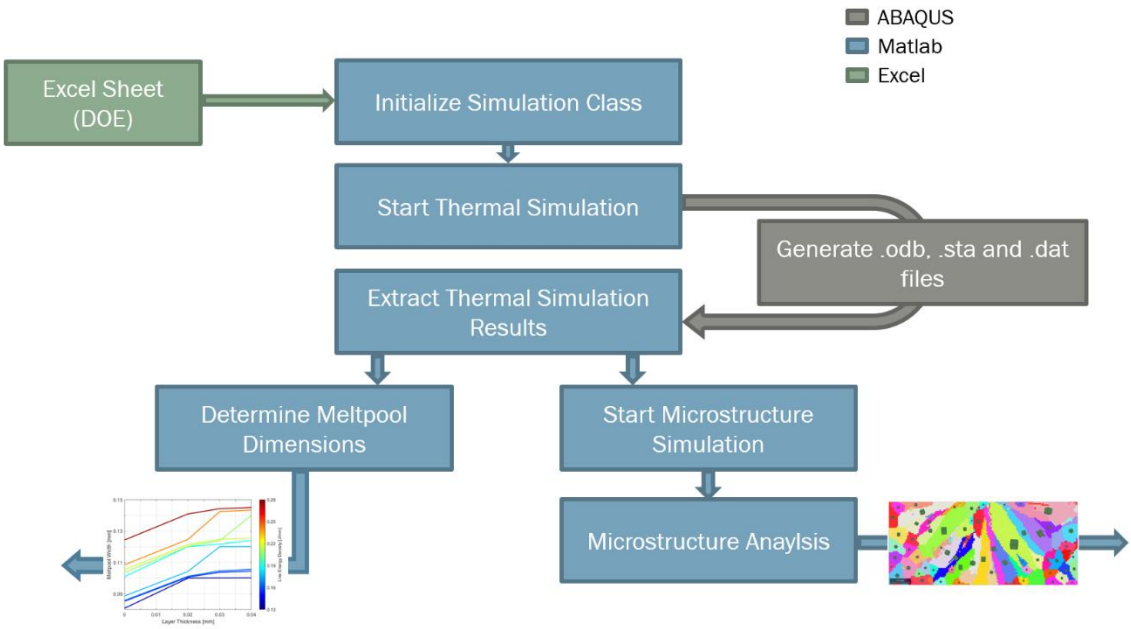

Figure 4.1 : Matlab Tool

4.2 Sensitivity Analysis to Process Parameters

One of the main tasks in this project is the sensitivity analysis to process parameter (P,t,v). For this purpose, a full factorial design of experiments with the discrete values of table 3.2 were performed. In a first step it was decided to visualize the sensitivity of the melt pool dimension to the energy density. Since these experiments are based on single track simulations the representative energy density was determined to be the line energy density (one-dimensional energy density):

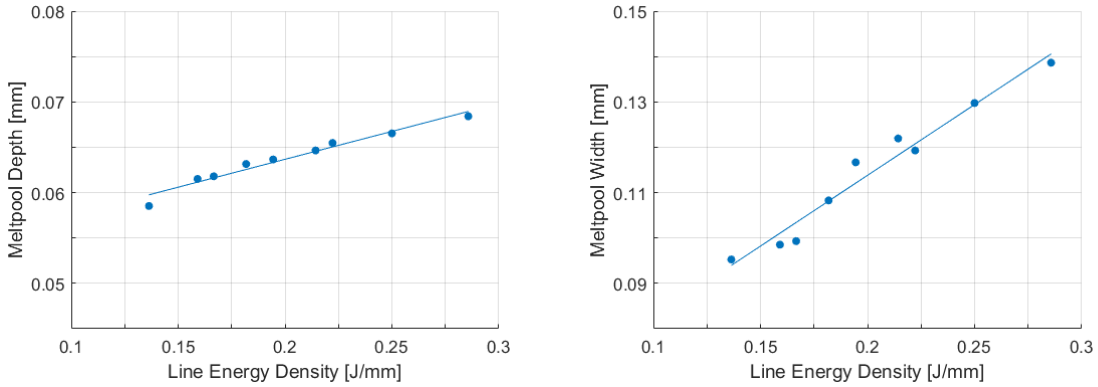

Figure 4.2 : Meltpool Depth and Width plotted against the Line Energy Density.

As expected, the melt pool dimensions increase with increasing line energy density. Higher line energy density corresponds to higher energy input into the system. Since the surrounding gas in SLM generally possesses low thermal conductivity, it is often modeled as being a thermal insulator. This means, the thermal energy must pass through the powder layer and the bulk material which explains why increasing energy densities lead to larger melt pool dimensions. On a second note, it is worth mentioning that the melt pool width seems to be affected stronger by an increase in line energy density. This can be explained by the fact that for the melt pool width there are two melting fronts while for the melt pool depth there is only one. Considering this fact, the change in melt pool width is still four times larger than the one of the melt pool depth.

As previously mentioned, the line energy density was chosen to be the representative energy density for these experiments. By definition, the line energy density only takes laser power P and laser scan speed v into account, see formulation in chapter 2.3. Thus, this analysis delivers no information of the impact of other parameters, like layer thickness t. In order to get a illustrative definition of this influence a secondary analysis was conducted. In this analysis

the layer thickness was plotted against the melt pool dimensions with different line energy density levels. The results of this analysis can be found in the following figure:

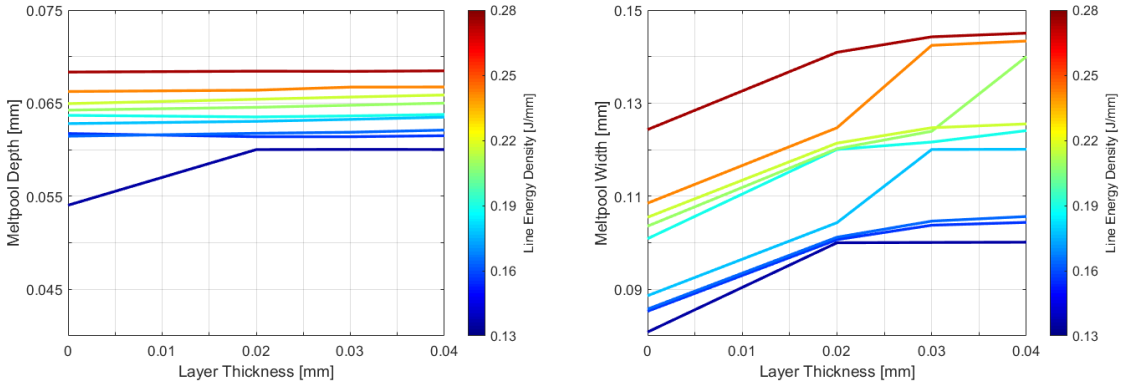

Figure 4.3 : Meltpool Width and Depth plotted against layer thickness for different line Energy Density levels.

From the above figures the previously defined trend is still visible, where increasing line energy densities lead to increasing melt pool dimensions. The left figure suggests that there is no distinct trend for the melt pool depth to change when increasing the layer thickness. On the right figure a clear secondary trend can be seen, where increasing layer thicknesses lead to wider melt pools. To stay consistent with the dimensions of the problem, where the melt pool depth has one melting front and the width has two, the scales of each plot were adjusted to satisfy the relation 2:1.

This secondary trend can be concluded by the fact that increasing layer thicknesses lead to lower overall thermal conductivity, since the powder has substantially lower thermal conductivity when compared to the bulk material. This reduction in thermal conductivity promotes localization of thermal energy in the vicinity of the heat source. With this localization of thermal energy, it is more likely that the temperature in the vicinity of the heat source will reach temperatures higher than their melting temperature. As a result, the melt pool width becomes larger.

The independence of melt pool depth to layer thickness is a byproduct of the modeling assumptions, in which vaporization effects were neglected. These are the main effects for the formation of keyhole phenomena, in which the melt pool is depressed (increasing the melt pool depth substantially).

4.3 Performance comparison between DOEs

For the generation of the metamodel two different DOEs were implemented and their performance was initially observed and compared. As previously mentioned, two error metrics were implemented, see **chapter 3.4.** The two chosen DOEs consist of Circumscribed Central Composite Design and Latin Hypercube Design. In a first step, an experiment plan was developed for each DOE. This plan consisted of 30 simulations each. For both approaches a Response Surface was generated and the errors were extracted. The following figure shows errors for each model:

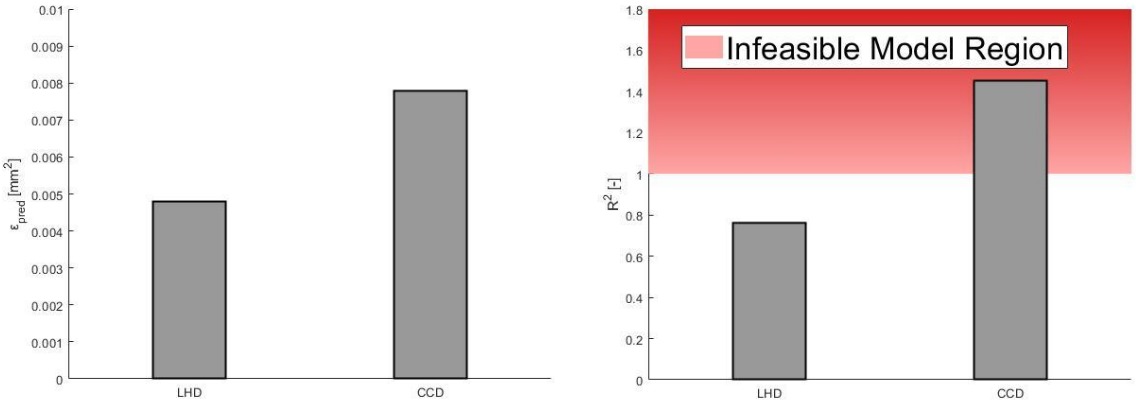

Figure 4.4 : (left) Prediction error model and (right) coefficient of multiple determination of each model.

The results from this analysis yielded that the model with Latin Hypercube sampling was outperforming the model with CCD in both categories. In the left figure it is evident that the LHD model possess lower prediction error when compared to the error of the CCD model. At the same time, the right figure suggests that the LHD model can predict almost 80% of the system' s variance while the CCD delivers infeasible results. If the coefficient of multiple determination is higher than 1 or negative, it is said that the model is unphysical and probably needs more design points to make a realistic prediction.

From this it was concluded that LHD is the superior approach for further investigation of the system since CCD requires much more design points than LHD in order to deliver representative results. It is still recommended to further investigate the properties of CCD since it commonly used in combination with RSM. In this project however, it was decided to drop the CCD due to time constraints.

4.4 Sensitivity Analysis to Modeling Parameters

The second main task of this project was the sensitivity analysis to modeling parameters, namely Goldak heat source parameters and absorptance. For validation of the obtained results and for the definition of a cost function, experimental data from A. Keshavarzkermani et al. [28] was used. Hereby the focus was set to one specific set of process parameters:

$$P = 200W, v = 1000\frac{mm}{s}, t = 0.04mm$$

For a general multidimensional system, it is advised to visualize the system's response in order to get an initially understanding of the system's behavior. Therefore, the modeling parameters were first plotted against a comparison term. This comparison term tries to encapsulate all parameters in one definition and provide information about the absorbed energy density:

$$C_1 = \frac{Absorptance}{Goldak\ Volume}$$

The generated plots can be found in the following figure:

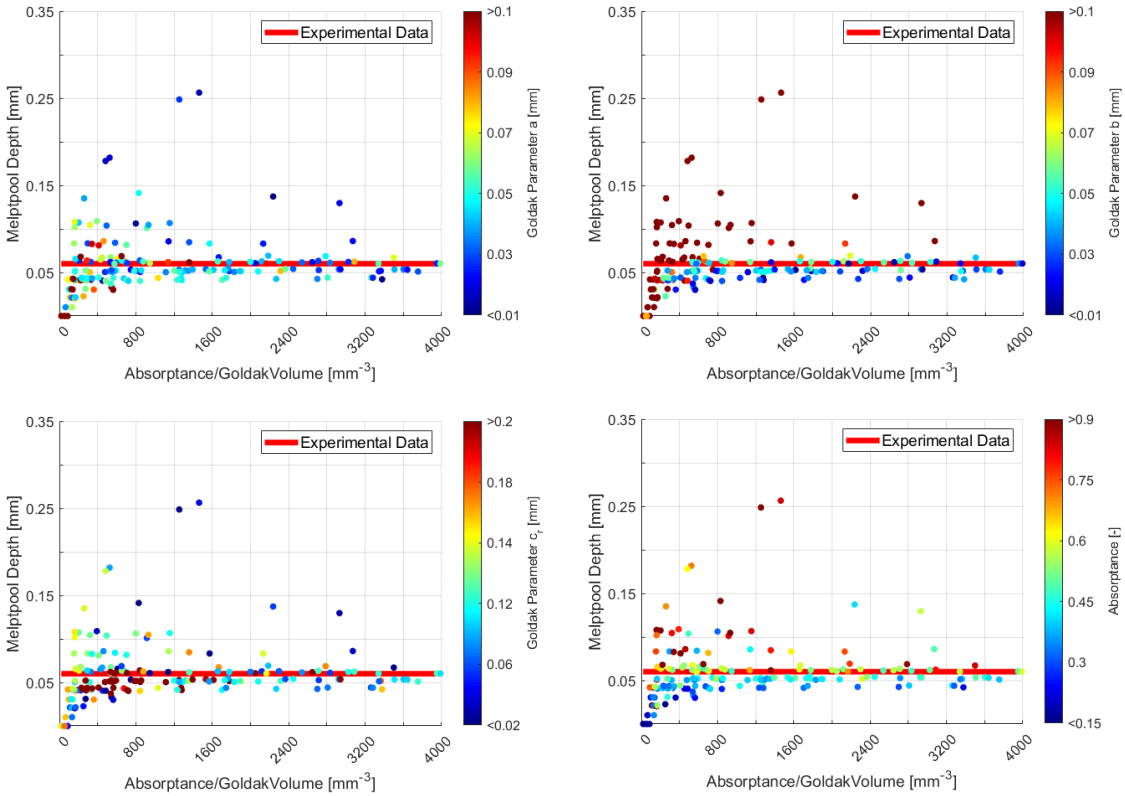

Figure 4.5 : Meltpool Depth plotted against absorbed energy density C_1 with colormap for (top left) Goldak Parameter a, (top right) Goldak Parameter b, (bottom left) Goldak parameter c_r and (bottom right) absorptance

If a parameter has a significant influence on the system' s response, there is a high chance for that parameter to show a trend in the previous figures. A trend can be characterized by the fact that similar parameter values consistently lead to similar responses. The analysis of these figures concluded that no distinct trend was observed for the Goldak parameter $\boldsymbol{a}$ and $\boldsymbol{c_r}$. On the other hand, it was concluded that there is a trend for the absorptance and Goldak parameter $\boldsymbol{b}$. This is consistent with the expectation that the depth parameter of the Goldak heat source model has a strong influence on the depth of the melt pool.

For $\boldsymbol{b}$ it is evident (from the top right graph in **figure 4.5**) that high values for $\boldsymbol{b}$ tend to consistently overpredict the melt pool depth or not form a melt pool at all, when combined with low values for the absorptance. At the same time low values for $\boldsymbol{b}$ tend to always underpredict the melt pool depth. For the absorptance a similar trend can be observed where low values consistently underpredict while high values consistently overpredict the melt pool depth.

For further investigation these parameters were plotted isolation where the absorbed energy density was reduced to a one-dimensional representation:

$$C_2 = \frac{Absorptance}{Goldak\ Parameter\ b}$$

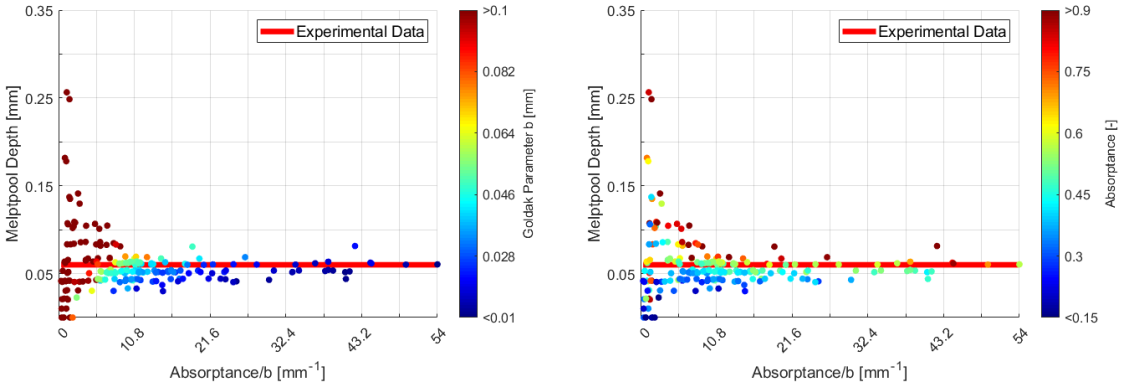

Figure 4.6 : Meltpool Depth plotted against the one-dimensional absorbed energy density $\boldsymbol{C_2}$ with colormap for (left) Goldak parameter b and (right) absorptance

In these figures a clear trend can be observed for $\boldsymbol{b}$. High values for $\boldsymbol{b}$ seem to have large scatter around the experimental data while lower levels for $\boldsymbol{b}$ seem to decrease the amount of scatter. At the same time, it can be seen that intermediate values for $\boldsymbol{b}$ [0.028-0.05] seem to produce the best results. From the right figure it is evident that the same trend is observed for the absorptance, where high values consistently overpredict melt pool depth while low values almost always

underpredict the melt pool depth. This can be attributed by the fact that higher values for the absorptance increase the captured thermal energy, which leads to overall higher energy density in the material. For the absorptance the optimal values seem to be in the range of [0.3-0.6].

The same procedure was implemented for the melt pool width with the following results with the absorbed energy density term C_1:

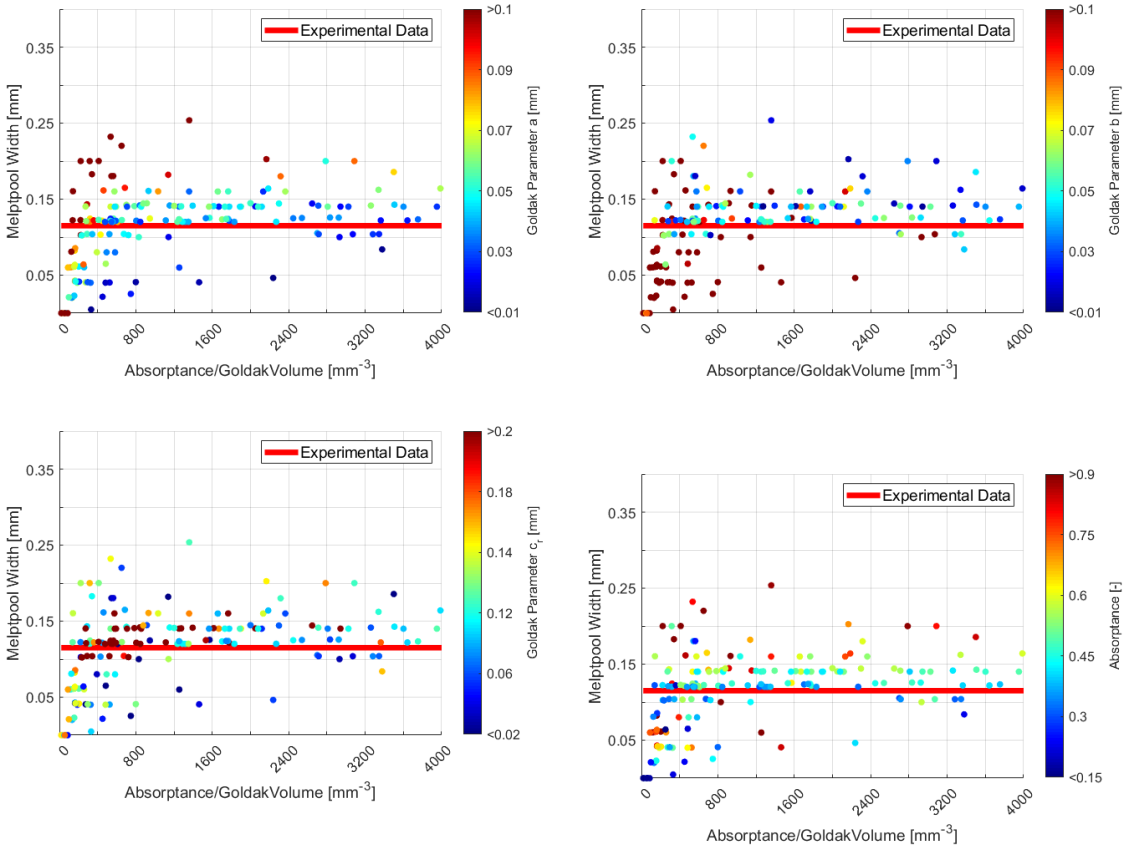

Figure 4.7 : Meltpool Width plotted against the absorbed energy density C_1 with colormap for (top left) Goldak Parameter a, (top right) Goldak Parameter b, (bottom left) Goldak parameter c_r and (bottom right)

The data for melt pool width seems to express higher scatter around the experimental data. Taking that into account, some clear trends can still be seen for the Goldak parameter a and the absorptance. Where high values for a tend to overpredict the meltpool width while low values underpredict the melt pool width. For the absorptance a weaker trend could be found where high values overpredict and low values underpredict the melt pool width. For the other two parameter no distinct trend could be observed and they were discarded as being not significant for the melt pool width.

For a deeper understanding of the relevant parameters, they were again plotted in isolation with the following one-dimensional absorbed energy density:

$$C_3 = \frac{Absorptance}{Golak\ Parameter\ a}$$

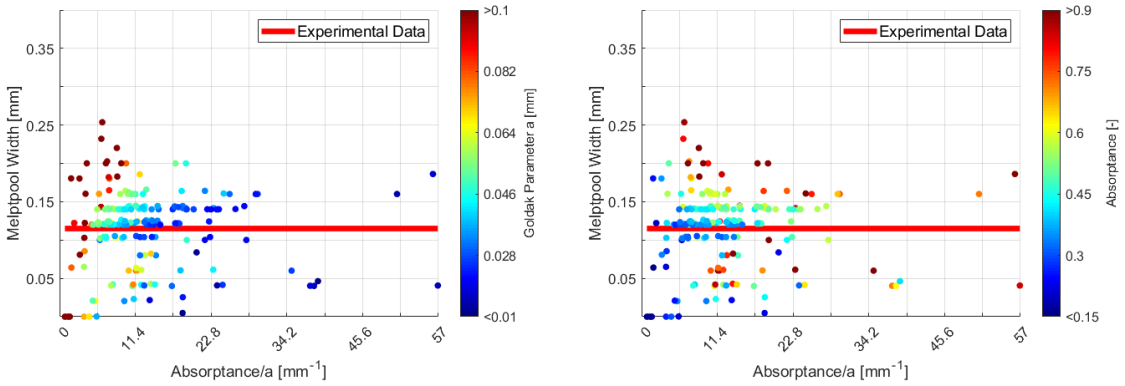

Figure 4.8 : Meltpool Width plotted against the one-dimensional absorbed energy density C_3 with colormap for (left) Goldak parameter a and (right) absorptance

In this visualization clear trends are visible for both parameters. For the Goldak parameter a high scatter is observed for high and low values, while low scatter is observed for medium values. For the absorptance a different trend is observed where the values in the lower range [0.3-0.4] seem to produce the best results while values above that threshold overpredict and values below that threshold underpredict the melt pool width.

The sensitivity analysis suggests a strong dependence of melt pool depth to the Goldak parameter b and absorptance. On the other hand, it also suggests a strong dependence of melt pool width to Goldak parameter a and absorptance. Both claims are consistence with the expected results, since both Goldak parameter are aligned with the measured directions. The observed scatter seemed to be higher in the melt pool width data as opposed to the melt pool depth data. No clear explanation for this difference in scatter level could be found. Additionally, the Goldak parameter c_r is suggested to not have any significant influence on the melt pool dimensions. This coincides with the expectation since no measurements on the melt pool length were conducted.

4.5 Optimization of relevant Modeling Parameters

For this part a response surface was created with the data gathered from the 220 simulations, which were sampled using the Latin Hypercube Design. The cost function used for the optimization was defined as follows:

$$Cost = |MD - EMD| + |MW - EMW|$$

Where MD denotes the measured melt pool depth, EMD the experimental melt pool depth, MW the measured melt pool width and EMW the experimental meltpool width.

In a first step the model was used to verify the claims made in the previous chapter. For this purpose, a full second order regression model was formulated using RSM and the P-Values of each term were plotted. The P-Value of a term represents the chance that this specific term has no significant influence on the system's response:

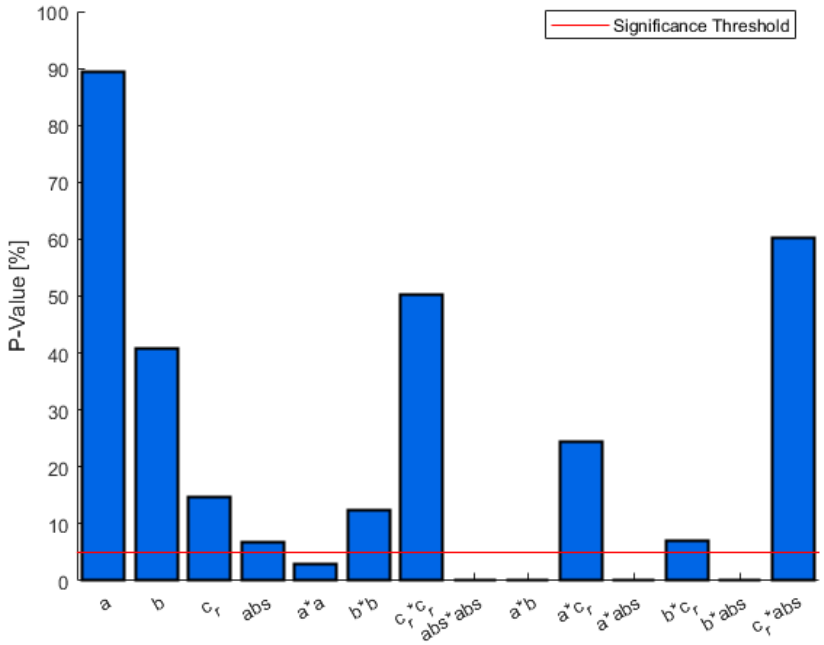

Figure 4.9 : P-Values for all terms in the full second order model with significance thershold at 5%.

From this figure it is evident all terms with c_r seem to have no significant influence on the system's response while higher order terms of a, b and absorptance seem to have very significant impact. The model also suggests a nonlinear relation between the system's response and the parameters a, b and absorptance. The figure also shows a tendency that the absorptance is the most

important parameter in the model. All these observations are consistent with the claims made in the previous chapter.

In a second step an optimization on the generated response surface was run. The optimization on the surface was broken down into multiple sub-optimizations and the results of these optimizations were then combined to give a hint for what values are expected to deliver optimal melt pool dimensions. The results of these optimizations are summarized in the following table:

Table 4.1: Optimized values for modeling parameters a, b, c_r and absorptance

Optimized Modeling Parameters			
a [mm]	b [mm]	c_r [mm]	absorptance [-]
[0.025-0.05]	[0.02-0.04]	Not Significant	[0.35-0.45]

These results are identical to the expected values obtained from the sensitivity analysis in the previous chapter.

5

5 Conclusion and Outlook

In this project the sensitivity of melt pool depth and width to process parameters and modeling parameters was conducted. From the sensitivity analysis to process parameters it could be concluded that increasing line energy densities lead to increasing melt pool depth and width. This result is consistent with the expectation that increasing energy leads to increasing melt pool dimensions. At the same time, since the line energy density carries no information about the dependence on layer thickness, another sensitivity analysis was performed. This analysis suggested that increasing layer thicknesses lead to increasing the melt pool widths while having no impact on the melt pool depth. The independence of the melt pool depth was attributed to the fact that vaporization phenomena and keyhole formation were neglected in this study. The other reason is that the absorptance was considered to be the same in the powder and dense material. The dependence of melt pool width to layer thickness was explained by the fact that increasing layer thicknesses lead to a reduction in the overall thermal conductivity of the system, which promotes localization of thermal energy in the vicinity of the heat source.

In the next step of the project a comparative study between Latin Hypercube Design and Circumscribed Central Composite Design was conducted and it was

concluded that the LHD exhibits superior performance. Furthermore, the CCD delivered infeasible results which hints that CCD requires more design points than LHD to yield representative results. This performance difference can be explained by the superior space filling properties of the Latin Hypercube Design.

In the sensitivity analysis to modeling parameters a strong dependance of melt pool depth to the Goldak parameter b and absorptance was observed. Furthermore, the meltpool width showed a strong dependence on the Goldak parameter a and absorptance. With visualization techniques clear trends of all relevant parameters were illustrated and optimal value assumption could be made.

For the validation of the claims made in the sensitivity analysis a metamodel was created using LHD and RSM techniques. The prediction of the significant variables made by this model coincides with the suggestions from the sensitivity analysis. In the last step, optimization was conducted on the response surface and the optimized values were consistent with the values obtained from the sensitivity analysis.

For future research it is suggested to change the thermal conductivity of the model from isotropic to fully anisotropic or to anisotropically enhanced, see [29]. Additionally, it is suggested to change the absorptance from a constant value to a temperature dependent value. Hereby the limits of the absorptance should be kept in the optimal range, while varying the temperature dependency terms. For the full quantification of such a complex problem a thorough investigation of DOE methods is suggested.

Bibliography

[1] L. Carter, Selective laser melting of nickel superalloys for high temperature applications, 2013

[2] G. Marchese et al., Study of the Microstructure and Cracking Mechanisms of Hastelloy X Produced by Laser Powder Bed Fusion, 2018

[3] Maria L. Montero-Sistiaga et al., Microstructure and mechanical properties of Hastelloy X produced byHP-SLM (high power selective laser melting),2019

[4] H. M. Tawancy, Long-term ageing characteristics of Hastelloy alloy X, 1983

[5] V. Griffiths et al., Cost-driven build orientation and bin packing of parts in Selective Laser Melting (SLM), 2019

[6] F. Wang, Mechanical property study on rapid additive layer manufacture Hastelloy® X alloy by selective laser melting technology, 2011

[7] S. Shrestha et al., A Study of Keyhole Porosity in Selective Laser Melting: Single-Track Scanning With Micro-CT Analysis, 2019

[8] W. E. King et al., Observation of keyhole-mode laser melting in laser powder-bed fusion additive manufacturing, 2014

[9] C. Panwisawas et al., Metal 3D printing as a disruptive technology for superalloys, 2020

[10] S. Pal et al., Evolution of the metallurgical properties of Ti-6Al-4V, produced with different laser processing parameters, at constant energy density in Selective Laser Melting, 2020

[11] K. Lee et al., A novel heat source model for analysis of melt Pool evolution in selective laser melting process, 2020

[12] T. Kik, Heat Source Models in Numerical Simulations of Laser Welding, 2020

[13] L. Binqi et al., A new ray tracing heat source model for mesoscale CFD simulation of selective laser melting (SLM), 2019

[14] J. Goldak et al., A new finite element model for welding heat sources, 1948

[15] X. Jin et al., Multiple Reflections and Fresnel Absorption of Gaussian Laser Beam in an Actual 3D Keyhole during Deep-Penetration Laser Welding, 2012
[16] A. V. Gusarov, Model of thermal conductivity in powder beds, 2009
[17] Y. R. Zhuang, Determination of melt pool dimensions using DOE-FEM and RSM with process window during SLM of Ti6Al4V powder, 2018
[18] U. Uhoraningoga et al., The Goldilocks Approach: A Review of Employing Design of Experiments in Prokaryotic Recombinant Protein Production, 2018
[19] Czitrom, V. (1999). One-Factor-at-a-Time versus Designed Experiments. The American Statistician, 53(2), 126—131. https://doi.org/10.2307/2685731
[20] J. A. Adepoju, R. A. Ipinyomi, Construction of Asymmetric Fractional Factorial Designs, 2016
[21] Wu, C. F. Jeff et al., Experiments: Planning, analysis, and parameter design optimization, 2000
[22] NIST/SEMATECH e-Handbook of Statistical Methods, http://www.itl.nist.gov/div898/handbook/, 2013
[23] N. R. Draper, Rotatable Design and Rotatability, 2008
[24] J. S. Park, Optimal Latin-hypercube designs for computer experiments, 1994
[25] Felipe A. C. Viana, Things you wanted to know about the Latin hypercube design and were afraid to ask, 2013
[26] Stander N., Roux W., Eggleston T., Craig K., LS-Opt User’s Manual. LSTC, 2006
[27] Myers, R.H., Montgomery, D.C. Response Surface Methodology. Process and Product Optimization using Designed Experiments. Wiley, 1995
[28] A. Keshavarzkermania et al., An investigation into the effect of process parameters on melt pool geometry, cell spacing, and grain refinement during laser powder bed fusion, 2019
[29] Sh. Safdar et al., An anisotropic enhanced thermal conductivity approach for modelling laser melt pools for Ni-base super alloys, 2013
[30] HASTELLOY® X alloy. http://haynesintl.com/docs/default-source/pdfs/newalloy-brochures/high-temperature-alloys/brochures/x-brochure.pdf?sfvrsn=15b829d4_40. Last visited: May 29, 2021.